

ОБЪЕДИНЕННЫЙ  
ИНСТИТУТ  
ЯДЕРНЫХ  
ИССЛЕДОВАНИЙ

Дубна

E13-2000-89

Yu.M.Gledenov, M.V.Sedysheva, G.Khuukhenkhuu<sup>1</sup>,  
Zhang Guohui<sup>2</sup>, Tang Guoyou<sup>2</sup>, Chen Jinxiang<sup>2</sup>,  
Zhang Xuemei<sup>3</sup>, Chen Zemin<sup>3</sup>, Chen Yingtang<sup>3</sup>

TWIN IONIZATION CHAMBER FOR STUDIES  
OF  $(n, p)$   $(n, \alpha)$  REACTIONS\*

---

\*The project supported by the National Natural Science Foundation of China and China National Nuclear Corporation and Russian Foundation for Basic Research, grant 96-02-10031, grant 98-02-17078

<sup>1</sup> Nuclear Research Center, National University of Mongolia, Ulaanbaatar, Mongolia

<sup>2</sup> Institute of Heavy Ion Physics, Peking University, Beijing, 100871, China

<sup>3</sup> Department of Physics, Tsinghua University, Beijing 100084, China

2000

## Introduction

Cross section data on neutron-induced charged-particle-emission reactions are of prime importance in evaluation of radiation damage and nuclear heating in reactors. However, at energies between 3 and 10 MeV, where the threshold of many charged particle emission reactions lie, the experimental data base is rather scarce and there are significant discrepancies of available results of various authors. In addition, previous measurements of these reactions in this energy range were made using activation techniques. This method, though easier in practice, is feasible only in certain cases where the residual nuclei reached by charged particle emission are unstable. Also, such measurements do not allow energy spectra and angular distributions to be obtained for the emitted charged particle. Though numerous charged particle detectors are developed and used in the neutron energy region of ~10-14 MeV, they are rarely used at energies <10 MeV because of their low solid-angle and counting efficiency.

In recent 7-8 years, we have successfully used a grid ionization chamber, in systematic studies of (n, $\alpha$ ) reactions [1-4]. The grid ionization chamber (GIC) has many advantages in charged particle measurements, such as the high geometrical efficiency, the capability of energy-angle determination and particle selection. In order to extend our investigations to (n,p) reactions, we have constructed a new twin GIC. It was designed at the Frank Laboratory of Neutron Physics, JINR, Dubna, Russia. The new GIC can bear higher gas pressures. In addition, the volume of the new GIC is smaller and this reduced the amount of the necessary working gas.

### 1. Twin Grid Ionization Chamber

Figure 1 shows the schematic structure of the chamber. The high gas pressure chamber has a cylindrical stainless steel shell 28.2 cm in diameter and 27.2 cm in height. It consists of two parallel sections with a common cathode. The anode plates are 0.1-0.2 mm thick aluminium foils. The grids consist of parallel gold-coated tungsten wires 0.1 mm in diameter spaced 2 mm apart.

Schematic view of cathode is shown in Fig.2. Samples are mounted on the rotating disk, fixed between two aluminium plates, that have the orifices 48 mm in diameter, which corresponds to the size of the samples. This construction allows only two samples to be expose. Since there are five positions on the rotating disk, ten samples, back to back, can be placed on it simultaneously, such as investigated samples, an  $\alpha$ -source, a background plate,  $^{238}\text{U}$  (to determinate the absolute neutron flux) etc. The rotating disk is connected with a knob outside the chamber by gear transmission. Therefore, during the experiment, it is possible to change the sample without changing working conditions in the GIC.

The anode and cathode signals for charged particles emitted from a sample placed on the cathode and stopped by the counting gas before reaching the Frisch grid can be represented by the equations [5]:

$$V_a = G_a E$$
$$V_c = G_c E \left( 1 - \frac{\bar{X}}{d} \cos \theta \right) \quad (1)$$

$$\cos \theta = \frac{d}{\bar{X}} \left( 1 - k_g (V_c / V_a) \right) \quad (2)$$

where  $V_c$ ,  $V_a$ ,  $G_c$ ,  $G_a$  are the cathode and anode signal pulse heights and the ratio constants, respectively,  $k_g = G_a / G_c$ ,  $E$  is the energy of the emitted charged particle,  $d$  is the spacing between the cathode and the Frisch-grid,  $\bar{X}$  is the distance from the origin to the center-of-gravity of the ionization track,  $\theta$  is the angle between the normal to the electrodes and the

particle track. Information about the energy and angle can be obtained from  $V_a$  and  $V_c$ , respectively.

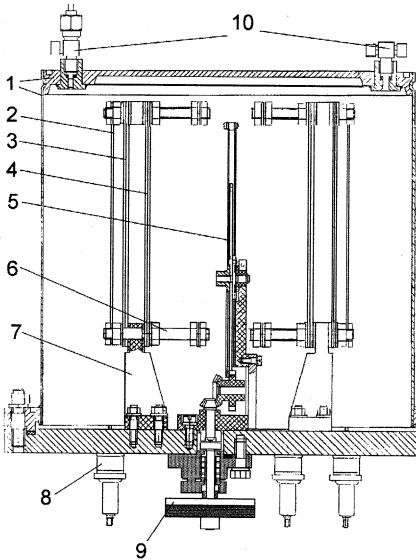


Fig. 1. Schematic view of the chamber.  
 1 - stainless steel shell, 2 - shield,  
 3 - anode, 4 - Frisch grid, 5 - cathode  
 6 - teflon spindle, 7 - teflon leg  
 8 - connectors, 9 - rotator, 10 - valve

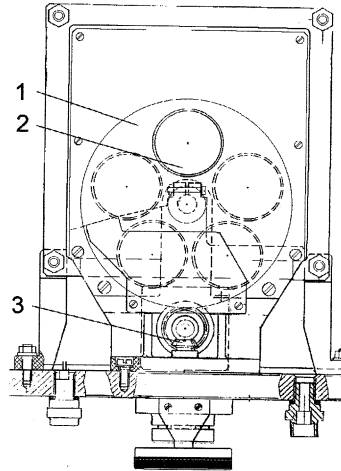


Fig. 2. Schematic view of cathode.  
 1 - rotating disk  
 2 - sample  
 3 - gear transmission

## 2. Experimental Set-up

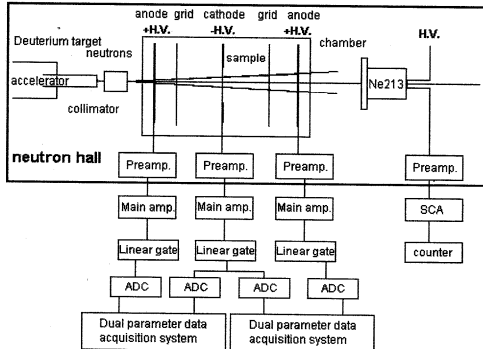


Fig. 3. Block diagram of the experimental setup.

Figure 3 shows the electronics of our experiment.

The diagram illustrates the output signals from the cathode and anodes of the chamber as they pass through preamplifiers, main spectroscopy amplifiers, delay line, linear gate,

analog-digital converter, two-dimensional data acquisition system and are received by computers. The anode and cathode signals can be obtained simultaneously. Then, two dimensional spectra of the emitted particles are obtained.

### 3. Investigations of the Working Conditions of the Chamber

We measure the anode pulse-height of  $\alpha$ -particles from an  $^{241}\text{Am}$  or  $\text{Pu}$   $\alpha$ -source (a compound  $\alpha$ -source of  $^{234}\text{U}$ ,  $^{238}\text{Pu}$ ,  $^{239}\text{Pu}$  and  $^{244}\text{Cm}$ ) and tritons from  $^6\text{Li}(n_{th},t)^4\text{He}$  as a function of  $E_{cg}/p$  at different pressures, where  $E_{cg}$  is the field strength between the cathode and the grid, and  $p$  is the pressure of the working gas. Figure 4 shows the saturation curves in krypton with 2.73%  $\text{CO}_2$ .

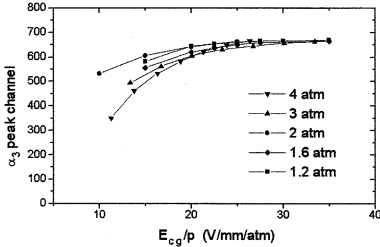


Fig. 4. Cathode saturation curve at different gas pressure

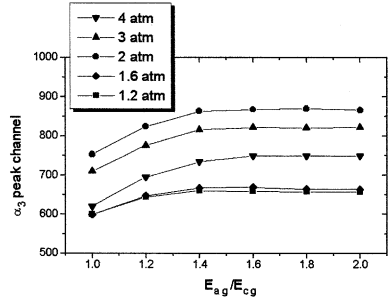


Fig. 5.  $E_{ag}/E_{cg}$  peak curve at different gas pressure

From the curves it is seen that the good working voltages  $E_{cg}$  is about 25-30 V/mm/atm. For argon with 3.78%  $\text{CO}_2$ , the required  $E_{cg}/p$  is just a little smaller (20-25 V/mm/atm).

Figure 5 illustrates the dependence of the peak position for the  $\alpha$ -source on the ratio of the field strength between the anode and the grid to the field strength between the grid and the cathode ( $E_{ag}/E_{cg}$ ) for an equal cathode voltage. Figure 5 shows that the optimum condition is  $E_{ag}/E_{cg} > 1.4$ . For the presented structure of the grid (parallel 0.1mm diameter wires 2 mm apart), it is 1.372 according to theoretical calculation. This value was 1.6-2.0 during our measurements.

The distance between the cathode and the grid is 45 mm and the distance between the grid and the anode is 25 mm. In such arrangement the grid shielding inefficiency is about 2.36%.

The gas pressure is determined from the range of the measured particles in the working gas and the cathode to grid distance. The pressure must be high enough to ensure that the particles are stopped before reaching the grid.

Using high voltage equipment ( $\pm 5000$  V) and krypton as a working gas, we can measure protons with the energy  $E_p$  up to 6 MeV and  $\alpha$ -particles with the energy  $E_\alpha$  up to 20 MeV.

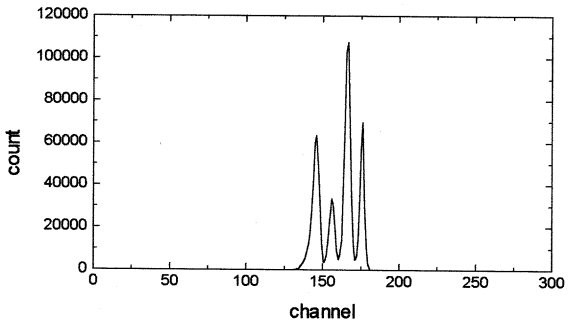


Fig. 6(a). Anode spectrum of  $\alpha$ - source.

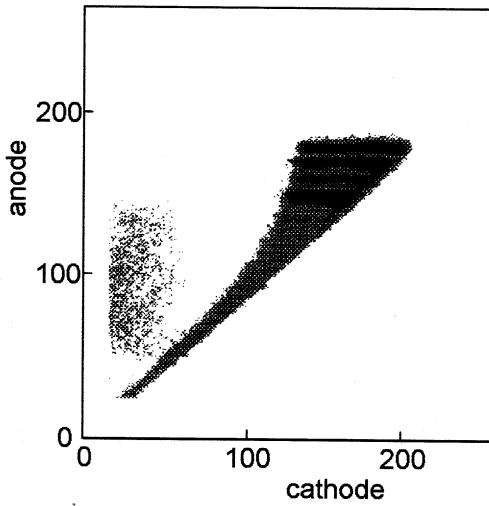


Fig. 6(b). Two-dimensional spectrum of compound  $\alpha$ -source.

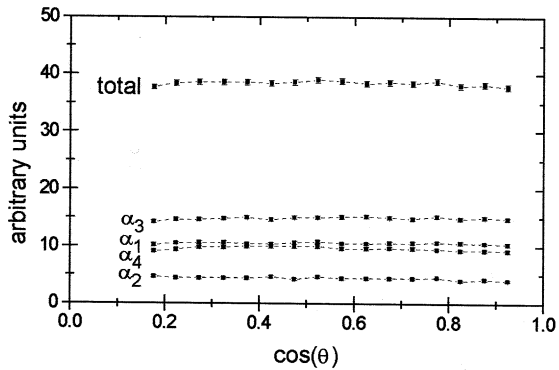


Fig. 6(c). Angular distribution of the  $\alpha$ -source.

In order to test the chamber, the energy spectra and angular distributions of a compound  $\alpha$  source ( $^{234}\text{U}$ ,  $^{238}\text{Pu}$ ,  $^{239}\text{Pu}$  and  $^{244}\text{Cm}$ ) and the recoil proton spectrum are measured. Figure 6 shows the two dimensional spectrum (a), and the corresponding anode spectrum (b) of the  $\alpha$  source at 1.2 atm in krypton. The energy resolution is about 2%. Figure 7(c) shows angular distributions of the  $\alpha$  source. In order to obtain the recoil proton spectrum, a polyethylene film was used as a target and it was bombarded with 4.1 MeV neutrons. The recoil proton anode spectrum (without background) in Fig. 7 is a rectangle as expected.

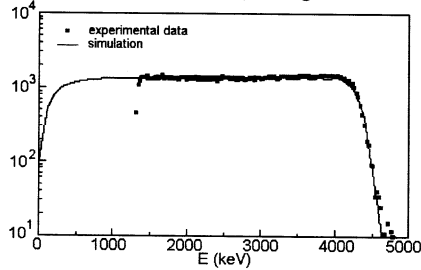


Fig. 7. Anode spectrum of recoil protons.

## 5. Experiments of (n, $\alpha$ ) and (n,p) Reactions

### 5.1. Experimental Arrangement

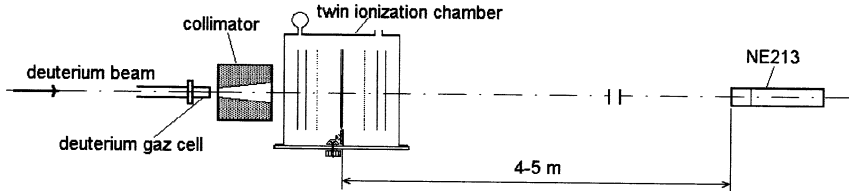


Fig. 8. Experimental arrangement.

The experiments were carried out at the 4.5 MV Van de Graaff Accelerator in Institute of Heavy Ion Physics in Peking University. Figure 8 shows the experimental arrangement. Nearly monoenergetic neutrons were produced via the  $\text{D}(n,d)\text{He}$  reaction using a deuterium gas cell. When it is filled with a 3 atm deuterium gas and the deuterium beam is 2-3  $\mu\text{A}$ , the neutron yield is about  $10^9/\text{s}$ . The NE213 liquid scintillation detector and a long counter ( $\text{BF}_3$ ) are used as relative neutron flux monitors. A  $^{238}\text{U}$  sample placed in the chamber was used to determine the absolute neutron flux.

### 5.2 Determination of Absolute Neutron Flux

The recoil proton spectrum can be used to determine the absolute neutron flux with Monte-Carlo simulation in (n,p) reactions. As a comparison, we used  $^{238}\text{U}$  as a target to determine the neutron flux in analogous conditions. A  $\text{BF}_3$  long counter was used as a relative neutron flux monitor in experiments. Results on the absolute neutron flux determined by different targets are normalized to  $\text{BF}_3$  count and are shown in Table 1.

Table 1. Comparison of measured neutron flux

	integrate neutron flux $\Phi_n$ (1/sr)		BF <sub>3</sub> count		$\Phi_n/\text{BF}_3$	
		error		error		error
polyethylene film	$2.05 \cdot 10^{11}$	3%	1692000	5%	$1.21 \cdot 10^5$	6%
<sup>238</sup> U	$1.33 \cdot 10^{12}$	3%	10862000	3%	$1.23 \cdot 10^5$	6%

In Table 1, the absolute neutron flux is determined with the help of a polyethylene film by calculation the recoil proton number and cross section of H(n,p) at 4.4 MeV. The flux determined with <sup>238</sup>U is calculated using the fission fragment number and cross section of <sup>238</sup>U (n,f) at 4.4 MeV. The results are in good agreement within the error range.

### 5.3 Energy Spectra, Angular Distribution and Cross Section Measurements

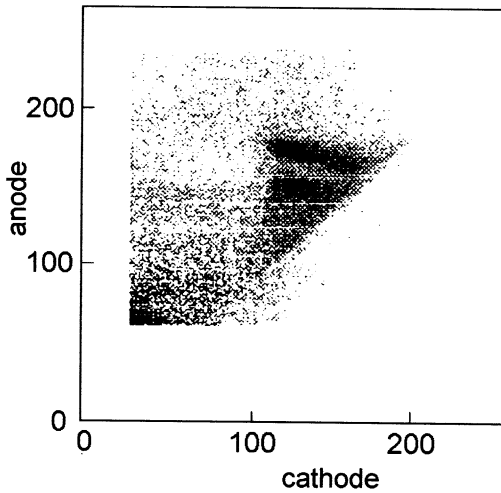


Fig. 9(a) Two-dimensional spectrum of <sup>39</sup>K(n,α)<sup>36</sup>Cl reaction at  $E_n=5.5$  MeV.

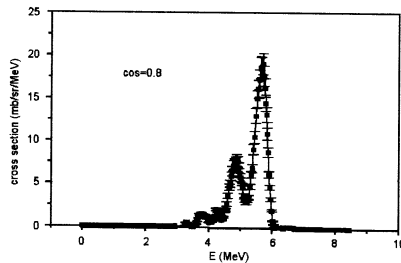


Fig. 9(b). Two differential cross sections of <sup>39</sup>K(n,α)<sup>36</sup>Cl at  $E_n=4.46 \pm 0.25$  MeV (36.9 degree, lab system).

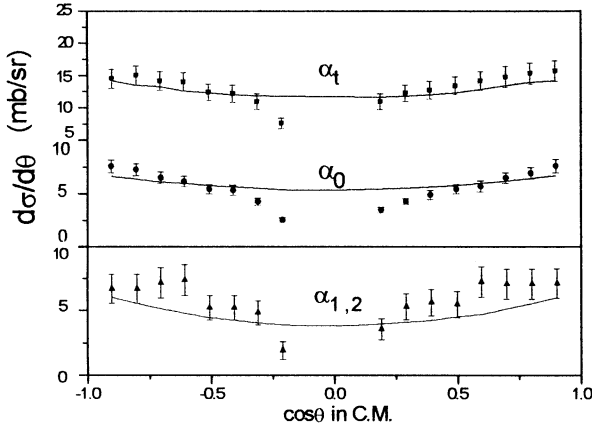


Fig. 9(c). The angular distribution of  $^{39}\text{K}(n,\alpha)^{36}\text{Cl}$  reaction at  $E_n=5.5$  MeV

Energy spectra, angular distributions and cross sections can be obtained from the measurement. Figure 9(a) shows the two-dimensional spectrum of  $\alpha$ -particles for the  $^{39}\text{K}(n,\alpha)^{36}\text{Cl}$  reaction at  $E_n=5.5\pm 0.2$  MeV. It can be clearly seen that there are two groups of particles; the first group corresponds to the ground state and the second to the first two excited states. Figure 9(b) shows two differential cross sections of  $^{39}\text{K}(n,\alpha)^{36}\text{Cl}$  at  $E_n=4.46\pm 0.25$  MeV (36.9 degree, lab system). Figure 9(c) shows the angular distributions of  $^{39}\text{K}(n,\alpha)^{36}\text{Cl}$  at  $E_n=5.5\pm 0.2$  MeV. The curve in this picture is fitting by  $y=a+bx+cx^2$  [6].

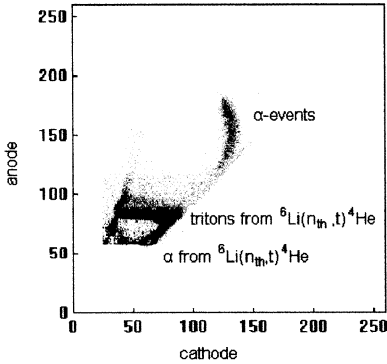


Fig. 10(a). The two-dimensional spectrum for forward (0-90°)  $\alpha$ -particles at  $E_n=3.67$  MeV

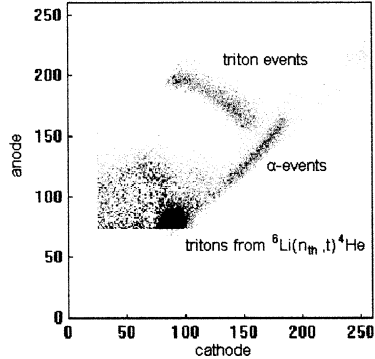


Fig. 10(b). The two-dimensional spectrum for forward (0-90°) triton measurement at  $E_n=4.42$  MeV.

Figure 10(a) is the two-dimensional spectrum for forward (0-90°)  $\alpha$ -particles at  $E_n=3.67$  MeV, from which the kinematical effect can be seen. Figure 10(b) shows the two-dimensional spectrum for forward (0-90°) triton measurement at  $E_n=4.42$  MeV.



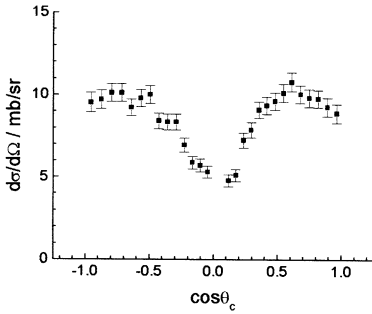


Fig. 11(a). The angular distribution for the  ${}^6\text{Li}(n,t){}^4\text{He}$  reaction at 3.67 MeV

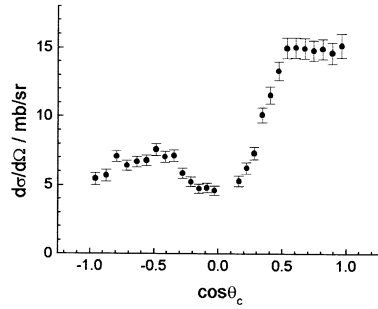


Fig. 11(b). The angular distribution for the  ${}^6\text{Li}(n,t){}^4\text{He}$  reaction at 4.42 MeV

Figures 11(a) and 11(b) illustrate the measured angular distributions for tritons at  $E_n=3.67$  and 4.42 MeV [7].

The experimental results have shown that the twin ionization chamber can be successfully used for studies of the  $(n,\alpha)$  and  $(n,p)$  reactions.

The authors wish to thank the van de Graaff accelerator laboratory for their help during the experiments and are also indebted to Prof. Xia Songjiang (Peking university, China, designer of double parameter data acquisition system), A.V.Androssov and Yu.N.Voronov (Dubna, JINR,Russia, constructor of GIC) and A.Zak (Lodz University, Lodz, Poland) for high voltage system discussion.

## References

1. Chen Ying-tang, Chen Ze-min, Qi Hui-quan et al. Angular Distribution and Cross Section Measurements of  ${}^{64}\text{Zn}(n,\alpha){}^{61}\text{Ni}$  Reaction for Neutron Energy 5 MeV. Chinese Journal of Nuclear Physics, 1995, v.17, No.2, p.167-170.
2. Tang Guoyou, Qu Decheng, Zhong Wenguang et al. Cross Section Measurements for  ${}^{40}\text{Ca}(n,\alpha){}^{37}\text{Ar}$  Reaction. Chinese Journal of Nuclear Physics, v.15, No.3, 1993, p.239-242.
3. Yu.M.Gledenov et al. Investigation of the Fast Neutron Induced  $(n,\alpha)$  Reaction (Experimental Techniques). Communications of the Joint Institute for Nuclear Research, E3-95-445, Dubna, 1995.
4. Yu.M.Gledenov et al. Cross Section and Angular Distribution Measurements of the Fast Neutron Induced  $(n,\alpha)$  Reaction for Medium-Mass Nuclei. Communications of the Joint Institute for Nuclear Research, E3-98-375, Dubna, 1998.
5. Knitter H.H., Budtz-Jørgensen C., Smith D.L. et al. Angular Distribution Measurements for the Reaction  $\text{Li}(n,t)\text{He}$ . Nucl.Sci.Eng., 1983, 83, p.229.
6. Xuemei Zhang et al. Measurements and Calculations of the  ${}^{39}\text{K}$  and  ${}^{40}\text{Ca}(n,\alpha)$  Cross Sections at  $E_n=4.5$  to 6.5 MeV. Nucl. Sci. Eng., 2000, 134, p.89-96.
7. Guohui Zhang et al. Differential Cross Sections Measurement for the  ${}^6\text{Li}(n,t){}^4\text{He}$  Reaction at 3.67 and 4.42 MeV. Nucl. Sci. Eng., 2000, 134, p.312-316.

Received by Publishing Department  
on April 19, 2000.

Гledenov Ю.М. и др.  
Двухсекционная ионизационная камера  
для исследования  $(n, p)$ -,  $(n, \alpha)$ -реакций

E13-2000-89

Для исследования реакций  $(n, p)$ ,  $(n, \alpha)$  на быстрых нейтронах была создана новая двухсекционная ионизационная камера. Были исследованы рабочие условия камеры. С помощью этой ионизационной камеры были получены энергетические спектры, угловые распределения и сечения  $(n, p)$ -,  $(n, \alpha)$ -реакций для ряда ядер.

Работа выполнена в Лаборатории нейтронной физики им. И.М.Франка ОИЯИ.

Сообщение Объединенного института ядерных исследований. Дубна, 2000

Gledenov Yu.M. et al.  
Twin Ionization Chamber for Studies of  $(n, p)$   $(n, \alpha)$  Reactions

E13-2000-89

For investigation of the fast neutron induced  $(n, p)$ ,  $(n, \alpha)$  reactions the new twin grid ionization chamber was constructed. The working conditions of the chamber were investigated. Using the ionization chamber, the energy spectra, angular distributions and cross sections of the  $(n, p)$ ,  $(n, \alpha)$  reactions were obtained for some nuclei.

The investigation has been performed at the Frank Laboratory of Neutron Physics, JINR.

Communication of the Joint Institute for Nuclear Research. Dubna, 2000